

Quark number densities at imaginary chemical potential in $N_f = 2$ lattice QCD with Wilson fermions and its model analyses

Junichi Takahashi,^{1,*} Hiroaki Kouno,^{2,†} and Masanobu Yahiro^{1,‡}

¹*Department of Physics, Graduate School of Sciences, Kyushu University, Fukuoka 812-8581, Japan*

²*Department of Physics, Saga University, Saga 840-8502, Japan*

(Dated: June 10, 2021)

We investigate temperature (T) dependence of quark number densities (n_q) at imaginary and real chemical potential (μ) by using $N_f = 2$ lattice QCD and the hadron resonance gas (HRG) model. Quark number densities are calculated at imaginary μ with lattice QCD on an $8^2 \times 16 \times 4$ lattice with the clover-improved $N_f = 2$ Wilson fermion action and the renormalization-group-improved Iwasaki gauge action. The results are consistent with the previous results of the staggered-type quark action. The n_q obtained are extrapolated to real μ by assuming the Fourier series for the confinement region and the polynomial series for the deconfinement region. The extrapolated results are consistent with the previous results of the Taylor expansion method for the reweighting factor. The upper bound $(\mu/T)_{\max}$ of the region where the extrapolation is considered to be reliable is estimated for each temperature T . We test whether T dependence of nucleon and Δ -resonance masses can be determined from LQCD data on n_q at imaginary μ by using the HRG model. In the test calculation, nucleon and Δ -resonance masses reduce by about 10% in the vicinity of the pseudocritical temperature.

PACS numbers: 11.15.Ha, 12.38.Gc, 11.30.Fs

I. INTRODUCTION

There are many interesting topics on quantum chromodynamics (QCD) at high density. The observation [1] of a two-solar-mass neutron star has an impact on the equation of state (EoS) of dense matter and the QCD phase diagram at high density. The experiments of relativistic heavy-ion collisions, for example the Beam Energy Scan experiments, are exploring QCD not only at finite temperature T but also at finite quark-chemical potential μ [2, 3]. Lattice QCD (LQCD) is the first-principle calculation to study QCD, but has the serious sign problem at finite μ .

In LQCD, the fermion determinant $\det M(\mu/T)$ becomes complex for finite real μ , because

$$(\det M(\mu/T))^* = \det M(-\mu^*/T) = \det M(-\mu/T). \quad (1)$$

This interferes with the use of Monte-Carlo simulations based on the importance sampling. For this reason, several methods were proposed so far in order to avoid the sign problem [4, 5]. Very recently, the complex Langevin method [6–9] and the Lefschetz thimble theory [10, 11] have attracted much attention as the method to go beyond $\mu/T = 1$.

One of the methods to avoid the sign problem is the imaginary- μ approach. For pure imaginary chemical potential $\mu = i\mu_I$, it is convenient to introduce the dimensionless chemical potential $\theta = \mu_I/T$. The first equality of Eq. (1) shows that the fermion determinant $\det M(i\theta)$ is real for imaginary μ . This makes LQCD simulations feasible there. Observables at real μ are extracted from those at imaginary μ by assuming functional forms for the observables.

In the imaginary μ region, QCD has two characteristic properties: one is the Roberge-Weiss (RW) periodicity and the other is the RW phase transition [12]. Figure 1 shows a schematic graph for the QCD phase diagram in the T - θ plane. The QCD grand partition function $Z(\theta)$ has a periodicity of $2\pi/N_c$ in θ :

$$Z(\theta) = Z\left(\theta + \frac{2\pi k}{N_c}\right), \quad (2)$$

where N_c is the number of colors and $k = 1, \dots, N_c$. This is a remnant of \mathbb{Z}_{N_c} symmetry in pure gauge theory and is now called the RW periodicity. Meanwhile, the RW transition is the first-order phase transition appearing at T higher than some temperature T_{RW} and $\theta = \pi/N_c$. This transition line and its \mathbb{Z}_{N_c} images are plotted by the solid lines in Fig. 1. The point located at $(T, \theta) = (T_{RW}, \pi/N_c)$ is called the RW endpoint. Meanwhile, the dashed line represents the transition line of confinement/deconfinement crossover. The pseudocritical temperature $T_c(\theta)$ is a function of θ , and the value at $\theta = 0$ [13] is denoted by T_{c0} . As shown later, T_{RW} is located between $1.08T_{c0}$ and $1.20T_{c0}$. The order parameter of the RW transition is a \mathcal{C} -odd quantity such as the phase of the Polyakov loop or the quark-number density [14], where \mathcal{C} means charge conjugation. The existence of the RW transition and the RW periodicity is numerically confirmed with LQCD simulations [15–20] and the underlying mechanism is clearly understood with the effective model [14, 21, 22] by introducing a new concept of extended \mathbb{Z}_{N_c} symmetry.

The quark number density n_q is a fundamental quantity to study high-density physics and important in determining the EoS at finite real μ . The EoS plays an essential role in investigating the structure of neutron stars. Moreover, n_q is useful to determine the strength of vector-type interaction in the effective model [23, 24]. For small real μ/T , the quark number density was calculated with the Taylor expansion method for the reweighting factor in which either the staggered-type [25] or the Wilson-type quark action [26] is

*takahashi@phys.kyushu-u.ac.jp

†kounoh@cc.saga-u.ac.jp

‡yahiro@phys.kyushu-u.ac.jp

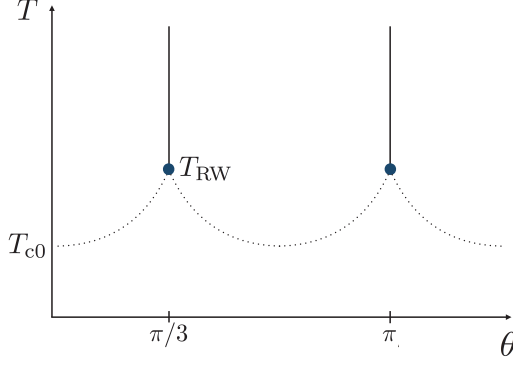


Fig. 1: QCD phase diagram in the imaginary μ region. The solid and dashed lines stand for the RW phase transition and the deconfinement crossover, respectively.

taken. The quark number density is also computed at imaginary μ in Refs. [17, 18, 27–29] with the staggered-type quark action, and n_q at real μ is deduced from that at imaginary μ by assuming analytic forms for n_q .

In this paper, we investigate μ dependence of n_q at both imaginary and real μ . We first perform LQCD simulations at imaginary μ with the Wilson-type quark action, since the quark number density at imaginary μ was not calculated with the Wilson-type quark action. LQCD simulations at imaginary μ do not require any special prescription in numerical calculations, since there is no sign problem. The n_q obtained at imaginary μ are extrapolated to the real μ region by assuming functional forms for n_q . The extrapolated results are confirmed to be consistent with the previous results [26] of the Taylor expansion method for the reweighting factor. The upper bound $(\mu/T)_{\max}$ of the region where the extrapolation is considered to be reliable is estimated for each T .

The hadron resonance gas (HRG) model is reliable in the confinement region. For the 2+1 flavor case at zero chemical potential, in fact, it is shown in Ref. [30] that the model well reproduces LQCD data on pressure at $T < 1.2T_{c0}$. As shown by the dashed line in Fig. 1, the pseudocritical temperature $T_c(\theta)$ of deconfinement transition *increases* from T_{c0} to T_{RW} as θ increases from zero to π/N_c . As for real μ , meanwhile, the pseudocritical temperature $T_c(\mu)$ *decreases* as μ increases. When μ varies from pure imaginary value to real value with T fixed at T_{c0} , the system is thus in the confinement phase for imaginary μ and in the deconfinement phase for real μ . Using this property, one can suggest that T dependence of nucleon and Δ -resonance masses in the vicinity of T_{c0} can be determined from n_q at imaginary μ by using the HRG model. We test how the suggestion works in this paper.

Actual LQCD simulations are done on an $8^2 \times 16 \times 4$ lattice with the clover-improved two-flavor Wilson fermion action and the renormalization-group-improved Iwasaki gauge action. We confirmed that the n_q calculated on an $8^2 \times 16 \times 4$ lattice are consistent with the previous results [18, 29] calcu-

lated on a $16^3 \times 4$ lattice. We then adopted an $8^2 \times 16 \times 4$ lattice to reduce simulation time and take more trajectories. We consider two temperatures $T/T_{c0} = 0.93$ and 0.99 in the confinement region and four temperatures $T/T_{c0} = 1.08, 1.20, 1.35$ and 2.07 in the deconfinement region. Following the previous LQCD simulation [26], we compute n_q along the line of constant physics at $m_{PS}/m_V = 0.80$, where m_{PS} and m_V are pseudoscalar- and vector-meson masses, respectively. This corresponds to the case of the pion mass $m_\pi \sim 616$ MeV and the quark mass $m_q \sim 130$ MeV [24] for $T_{c0} \sim 171$ MeV [31]. The analytic continuation is carried out with the Fourier series for $T < T_{c0}$ and the polynomial series for $T > T_{RW}$.

This paper is organized as follows. In Sec. II, we explain the lattice action, the quark number density and the analytic continuation. In Sec. III, we show our simulation parameters and numerical results for n_q at both imaginary and real μ . In Sec. IV, we test whether T dependence of nucleon and Δ -resonance masses can be determined from LQCD data on n_q at imaginary μ by using the HRG model. Section V is devoted to a summary.

II. FORMULATION

A. Lattice action

We use the renormalization-group-improved Iwasaki gauge action S_g [32] and the clover-improved two-flavor Wilson quark action S_q [33] defined by

$$S = S_g + S_q, \quad (3)$$

$$S_g = -\beta \sum_x \left(c_0 \sum_{\mu < \nu; \mu, \nu=1}^4 W_{\mu\nu}^{1 \times 1}(x) + c_1 \sum_{\mu \neq \nu; \mu, \nu=1}^4 W_{\mu\nu}^{1 \times 2}(x) \right), \quad (4)$$

$$S_q = \sum_{f=u,d} \sum_{x,y} \bar{\psi}_x^f M_{x,y} \psi_y^f, \quad (5)$$

where $\beta = 6/g^2$ for the gauge coupling g , $c_1 = -0.331$, $c_0 = 1 - 8c_1$, and

$$M_{x,y} = \delta_{xy} - \kappa \sum_{i=1}^3 \{ (1 - \gamma_i) U_{x,i} \delta_{x+\hat{i},y} + (1 + \gamma_i) U_{y,i}^\dagger \delta_{x,y+\hat{i}} \} - \kappa \{ e^{\hat{\mu}} (1 - \gamma_4) U_{x,4} \delta_{x+\hat{4},y} + e^{-\hat{\mu}} (1 + \gamma_4) U_{y,4}^\dagger \delta_{x,y+\hat{4}} \} - \delta_{xy} c_{SW} \kappa \sum_{\mu < \nu} \sigma_{\mu\nu} F_{\mu\nu}. \quad (6)$$

Here κ is the hopping parameter, $\hat{\mu}$ is the quark chemical potential in lattice units, and the lattice field strength $F_{\mu\nu}$ is defined as $F_{\mu\nu} = (f_{\mu\nu} - f_{\mu\nu}^\dagger)/(8i)$ with $f_{\mu\nu}$ the standard clover-shaped combination of gauge links. For the clover coefficient c_{SW} , we take the mean-field value estimated from $W^{1 \times 1}$ in the one-loop level: $c_{SW} = (W^{1 \times 1})^{-3/4} =$

$(1 - 0.8412\beta^{-1})^{-3/4}$ [32]. The value of κ is determined at $\mu = 0$ for each β along the line of constant physics with $m_{\text{PS}}/m_V = 0.80$ [31, 34, 35].

B. Quark number density

The quark number density n_q is defined as

$$\frac{n_q}{T^3} = \frac{1}{VT^2} \frac{\partial}{\partial \mu} \ln Z \quad (7)$$

$$= \frac{N_f N_t^3}{N_V} \text{tr} \left[M^{-1} \frac{\partial M}{\partial \hat{\mu}} \right], \quad (8)$$

where V is the volume, N_f is the number of flavors, N_t is the temporal lattice size, N_V is the lattice volume and M is the fermion matrix. We apply the random-noise method for the trace in Eq. (8). The number of noise vectors is about 4,000. The partition function Z is μ -even (\mathcal{C} -even), so that n_q is μ -odd (\mathcal{C} -odd) from Eq. (7). This means that n_q is pure imaginary for imaginary μ ; actually,

$$n_q^* = \left(\frac{1}{V} \frac{\partial \ln Z}{\partial (i\theta)} \right)^* = \frac{1}{V} \frac{\partial \ln Z}{\partial (-i\theta)} = -n_q. \quad (9)$$

We have confirmed in our LQCD simulations that the real part of n_q is zero at imaginary μ . For later convenience, we represent the imaginary part of n_q by n_q^I : $n_q^I = \text{Im}(n_q)$.

C. Analytic continuation

Our final interest is n_q at real μ . We then extrapolate the n_q calculated at imaginary μ with LQCD to the real μ region, assuming some functional forms for n_q . As for the pseudo-critical line, it is shown in Refs. [20, 36–38] that the terms of order higher than μ^2 are necessary.

In the imaginary- μ region, n_q is a θ -odd function with the RW periodicity. We then consider only a period $-\pi/3 < \theta \leq \pi/3$ for simplicity. In the confinement region at $T < T_{c0}$, the quark number density is smooth for any θ , indicating that $n_q = 0$ at $\theta = 0, \pm\pi/3$ [14, 21, 22]. Hence n_q can be described with good accuracy by a partial sum $S_F^n(T, \theta)$ of the Fourier series:

$$\frac{n_q(T, i\theta)}{T^3} \approx i S_F^n(T, \theta) = i \sum_{k=1}^n a_F^{(k)}(T) \sin(3k\theta) \quad (10)$$

where the superscript n of $S_F^n(T, \theta)$ represents the highest order in the partial sum. The coefficients $a_F^{(k)}(T)$ are obtained by fitting the function (10) to LQCD data at imaginary $\mu = i\mu_I$. The analytic continuation from $\mu = i\mu_I$ to $\mu = \mu_R$ can be made by replacing $i\mu_I/T$ by μ_R/T in Eq. (10):

$$\begin{aligned} \frac{n_q(T, \mu_R/T)}{T^3} &\approx g_F^n \left(T, \frac{\mu_R}{T} \right) \\ &= \sum_{k=1}^n a_F^{(k)}(T) \sinh \left(3k \frac{\mu_R}{T} \right). \end{aligned} \quad (11)$$

Here note that the coefficients $a_F^{(k)}(T)$ have already been determined at imaginary μ .

In the region $T_{c0} < T < T_{\text{RW}}$, the system is in the deconfinement region for small θ but in the confinement region for large θ near $\pi/3$, as shown in Fig. 1. Because of this property, the θ dependence of n_q is complicated and makes the analytic continuation difficult. We then do not perform the analytic continuation in this region.

In the deconfinement region at $T > T_{\text{RW}}$, the quark number density is discontinuous at $\theta = \pm\pi/3$ where the first-order RW phase transition takes place; note that n_q is the order parameter of the RW first-order transition [14]. Owing to this property, n_q monotonically increases with θ , as shown later in Fig. 2. This suggests that n_q can be described with good accuracy by a partial sum $S_p^{2n-1}(T, \theta)$ of the polynomial series:

$$\frac{n_q(T, i\theta)}{T^3} \approx i S_p^{2n-1}(T, \theta) = i \sum_{k=1}^n a_p^{(2k-1)}(T) \theta^{2k-1}, \quad (12)$$

where the superscript n of $S_p^{2n-1}(T, \theta)$ represents the highest order in the partial sum. Again, the analytic continuation is made by replacing $i\mu_I/T$ by μ_R/T in Eq. (12):

$$\begin{aligned} \frac{n_q(T, \mu_R/T)}{T^3} &\approx g_p^{2n-1} \left(T, \frac{\mu_R}{T} \right) \\ &= \sum_{k=1}^n (-1)^{(k-1)} a_p^{(2k-1)}(T) \left(\frac{\mu_R}{T} \right)^{2k-1}. \end{aligned} \quad (13)$$

III. NUMERICAL RESULTS

Full QCD configurations with $N_f = 2$ dynamical quarks were generated with the hybrid Monte-Carlo algorithm on a lattice of $N_x \times N_y \times N_z \times N_t = 8^2 \times 16 \times 4$. The step size of the molecular dynamics is $\delta\tau = 0.02$ and the step number is $N_\tau = 50$. The acceptance ratio is more than 95%. We generated about 32,000 trajectories and removed first 4,000 trajectories for the thermalization of all the parameters, and measured n_q at every 100 trajectories. The relation of parameters κ and β to the corresponding T/T_{c0} was determined in Refs. [31, 34, 35]; see Table I for the relation.

A. Quark number density at imaginary μ

Figure 2 shows n_q^I/T^3 as a function of θ for all the temperatures we consider. The LQCD data are plotted by symbols with error bars, although the errors are quite small. The number density n_q^I should be zero at $\theta = \pi/3$ below T_{RW} but finite above T_{RW} , since n_q^I is the order parameter of the first-order RW phase transition. One can see from this fact that T_{RW} is located between $1.08T_{c0}$ and $1.2T_{c0}$. The quark number density n_q^I/T^3 behaves as the sine function for $T < T_{c0}$, but monotonically increases up to $\theta = \pi/3$ for $T > T_{\text{RW}}$. As for $T = 1.08T_{c0}$, the system is in the deconfinement region for $\theta < 0.8$ but in the confinement region for $0.8 < \theta < \pi/3$,

κ	β	T/T_{c0}
0.141139	1.80	0.93(5)
0.140070	1.85	0.99(5)
0.138817	1.90	1.08(5)
0.137716	1.95	1.20(6)
0.136931	2.00	1.35(7)
0.135010	2.20	2.07(10)

TABLE I: Summary of the simulation parameter sets determined in Refs. [31, 34, 35]. Note that $T_{c0} \simeq 171\text{MeV}$, where T_{c0} is the pseudocritical temperature of deconfinement transition at $\mu = 0$. In the parameter setting, the lattice spacing a is about $0.14 \sim 0.2$ fm.

since n_q^I/T^3 increases monotonically up to $\theta \sim 0.7$ but decreases to zero for $\theta > 0.8$. This result is consistent with that of the staggered-type fermion in Ref. [29]. The present result is thus independent of the fermion action taken.

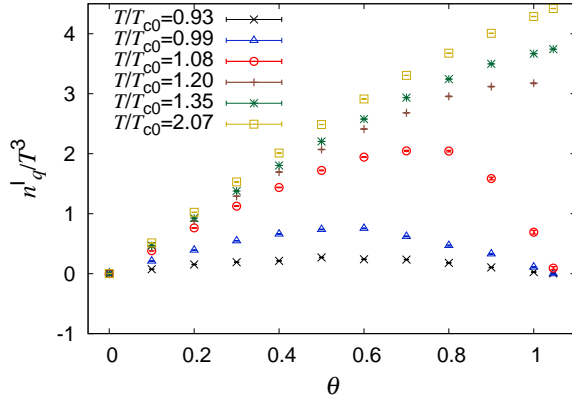


Fig. 2: μ_1/T dependence of n_q^I/T^3 at various values of T . The LQCD data are shown by symbols with error bars, although the error bars are quite small.

First we consider the case of $T < T_{c0}$ and determine the coefficients $a_F^{(k)}(T)$ of the Fourier series from the n_q calculated at imaginary μ with LQCD. In principle, n_q is described as an infinite series of sine functions for imaginary μ and of hyperbolic sine functions for real μ , as shown in Eqs. (10) and (11). The partial sum is valid only when the series converges. Particularly for real μ , the hyperbolic sine functions increase rapidly as μ/T becomes large. In this sense, it is important that the coefficients $a_F^{(k)}$ becomes small rapidly as k increases.

In Fig. 3, the results of χ^2 fitting are compared with the LQCD results. Here, two cases of S_F^1 and S_F^2 are plotted by dashed and solid curves, respectively. The two results well reproduce the LQCD data.

The coefficients obtained are tabulated in Table II for three cases of S_F^1 , S_F^2 and S_F^3 and two cases of $T = 0.93T_{c0}$ and

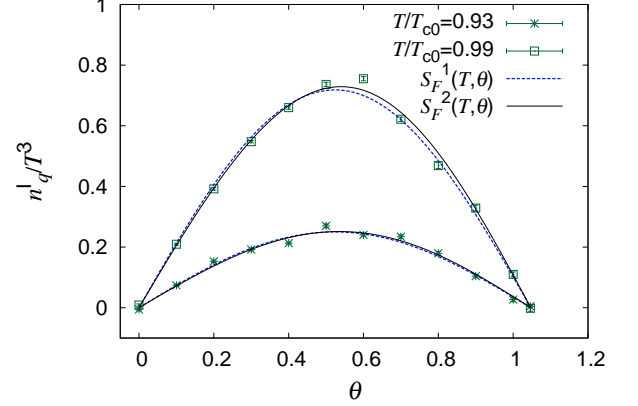


Fig. 3: Results of χ^2 fitting to LQCD data for the case of $T < T_{c0}$. The results of S_F^1 and S_F^2 are plotted by dashed and solid lines, respectively. LQCD data are shown by symbols with error bars.

$0.99T_{c0}$, together with the values of χ^2 per degree of freedom (d.o.f.). As for $T = 0.93T_{c0}$, the absolute value of $a_F^{(2)}$ is much smaller than $a_F^{(1)}$ in S_F^2 , but $a_F^{(3)}$ is comparable to the absolute value of $a_F^{(2)}$ in S_F^3 . In addition, the $\chi^2/\text{d.o.f.}$ value little changes between S_F^2 and S_F^3 . The result of S_F^2 is thus acceptable, but that of S_F^3 is not. Similar discussion is possible for $T = 0.99T_{c0}$; note that the absolute value of $a_F^{(2)}$ is comparable to that of $a_F^{(3)}$ in S_F^3 if the error ranges of $a_F^{(2)}$ and $a_F^{(3)}$ are taken into account. As shown in Fig. 3, moreover, the deviation of LQCD data from the solid line (the result of S_F^2) is rapidly oscillating with θ and cannot be reproduced by the next-order term $\sin(9\theta)$. Thus the coefficients higher than $a_F^{(2)}$ may not be determined from the present LQCD data. We then consider S_F^1 and S_F^2 as the extrapolation function from imaginary μ to real μ .

Next we consider the case of $T > T_{RW}$ and determine the coefficients $a_p^{(2k-1)}(T)$ of the polynomial series. In Fig. 4, the fitting results are compared with LQCD data for S_p^3 in panel (a) and for S_p^5 in panel (b). For each case of $T = 1.20T_{c0}$, $1.35T_{c0}$ and $2.07T_{c0}$, two dashed lines stand for the upper and lower bounds of χ^2 fitting, respectively. The fitting results well reproduce LQCD data. The resulting coefficients $a_p^{(2k-1)}(T)$ are tabulated in Table III for three cases of S_p^3 , S_p^5 and S_p^7 , together with the $\chi^2/\text{d.o.f.}$ values. For each temperature, S_p^7 has the smallest $\chi^2/\text{d.o.f.}$ value among S_p^3 , S_p^5 and S_p^7 . Particularly at $T = 1.35T_{c0}$, the value is almost one. Nevertheless, for each temperature the absolute value of $a_p^{(7)}$ is comparable to that of $a_p^{(5)}$ in S_p^7 , whereas the absolute value of $a_p^{(5)}$ is smaller about by an order of magnitude than that of $a_p^{(3)}$ in S_p^5 . We also performed a fit with ratios of polynomials to take account of the terms of order higher than $a_p^{(7)}$, following Ref. [37]. The resulting $\chi^2/\text{d.o.f.}$ value is much

larger than the case of S_p^7 . This may indicate that $a_p^{(7)}$ and its higher-order coefficients cannot be determined properly from

the present LQCD data. We then use S_p^3 and S_p^5 as the extrapolation function from imaginary μ to real μ .

T/T_{c0}	$a_F^{(1)}$	$a_F^{(2)}$	$a_F^{(3)}$	$\chi^2/\text{d.o.f.}$	$\mu_1/T(\text{fitting range})$
0.93	0.250(2)			5.937	$0 \sim \pi/3$
0.93	0.251(2)	-0.00457(216)		6.084	$0 \sim \pi/3$
0.93	0.251(2)	-0.00526(219)	0.00440(214)	6.290	$0 \sim \pi/3$
0.99	0.718(2)			11.06	$0 \sim \pi/3$
0.99	0.728(3)	-0.0179(26)		7.453	$0 \sim \pi/3$
0.99	0.727(3)	-0.0137(30)	-0.00825(276)	7.288	$0 \sim \pi/3$

TABLE II: Coefficients of the Fourier series for S_F^1 , S_F^2 and S_F^3 .

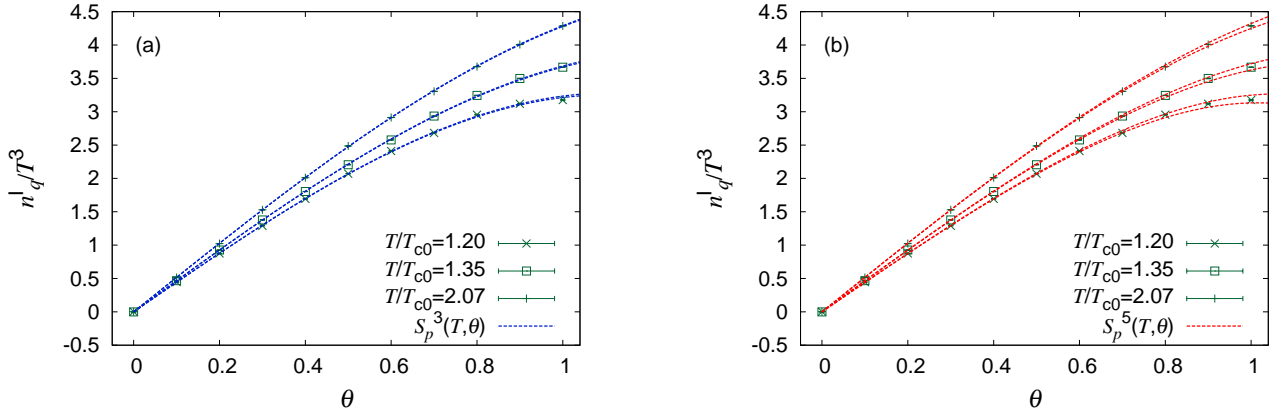


Fig. 4: Results of χ^2 fitting to LQCD data for the case of $T > T_{RW}$. Panels (a) and (b) show the results of S_p^3 and S_p^5 , respectively. For each temperature, two dashed lines correspond to the upper and lower bounds of the χ^2 fitting, respectively. LQCD data are shown by symbols with error bars.

T/T_{c0}	$a_p^{(1)}$	$a_p^{(3)}$	$a_p^{(5)}$	$a_p^{(7)}$	$\chi^2/\text{d.o.f.}$	$\mu_1/T(\text{fitting range})$
1.20	4.437(4)	-1.214(7)			13.66	$0 \sim 1$
1.20	4.407(5)	-1.024(27)	-0.1935(260)		8.472	$0 \sim 1$
1.20	4.427(7)	-1.274(66)	-0.4458(1569)	-0.4229(1024)	7.245	$0 \sim 1$
1.35	4.675(3)	-0.9973(49)			6.036	$0 \sim 1$
1.35	4.662(5)	-0.9223(223)	-0.06736(1956)		5.308	$0 \sim 1$
1.35	4.695(7)	-1.295(67)	-0.7986(1469)	-0.5310(893)	1.011	$0 \sim 1$
2.07	5.174(2)	-0.8904(40)			9.161	$0 \sim 1$
2.07	5.177(4)	-0.9056(177)	0.01356(1531)		10.21	$0 \sim 1$
2.07	5.158(6)	-0.7119(432)	0.4381(932)	0.2819(574)	8.220	$0 \sim 1$

TABLE III: Coefficients of the polynomial series for S_p^3 , S_p^5 and S_p^7 .

B. Quark number density at real μ

g_F^1 and g_F^2 . Figure 5 shows μ/T dependence of n_q/T^3 for

First we consider the case of $T/T_{c0} < 1$. As the extrapolation function from imaginary μ to real μ , we consider

$T = 0.99T_{c0}$. The result of the extrapolation is shown by a pair of lines; the two lines correspond to the upper and lower bounds of the extrapolation and the uncertainty comes from the errors in $a_F^{(k)}$. The g_F^2 case (solid line) has a larger error than the g_F^1 case (dashed line), because the former error comes from both of $a_F^{(1)}$ and $a_F^{(2)}$ but the latter does from $a_F^{(1)}$ only. We also show the previous LQCD result [26] of the Taylor expansion method for the reweighting factor by symbols with error bars. In the previous calculation, n_q is described by a polynomial series of μ/T and the terms up to $(\mu/T)^3$ are taken into account. The result of g_F^2 deviates from that of the Taylor expansion method at $\mu/T > 0.8$. To clarify what causes the deviation, in Eq. (11) for g_F^2 we expand the hyperbolic sine function into a polynomial series and discard the terms of order higher than $(\mu/T)^3$. We denote the resulting function by \bar{g}_F^2 . The result of \bar{g}_F^2 (dotted line) is consistent with that of the Taylor expansion method at $\mu/T < 1$. Thus the difference between g_F^2 and the Taylor expansion method comes from the terms of order higher than $(\mu/T)^3$, and g_F^2 yields a correction to the result of the Taylor expansion. From the fact that the correction is small at $\mu/T < 0.8$, we can conclude that both the previous result of the Taylor expansion method and the present result of g_F^2 are reliable at least at $\mu/T < 0.8$.

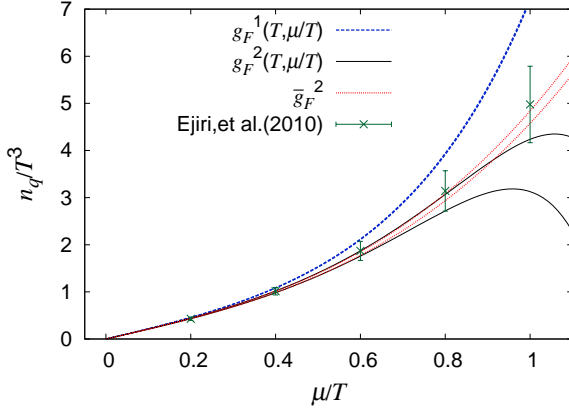


Fig. 5: μ/T dependence of n_q/T^3 at $T = 0.99T_{c0}$. The results of g_F^1 , g_F^2 and \bar{g}_F^2 are plotted by dashed, solid and dotted lines, respectively; see the text for the definition of \bar{g}_F^2 . For each case, the upper and the lower bounds of χ^2 fittings are shown by a pair of lines. The symbols denotes LQCD results of the Taylor expansion method for the reweighting factor in Ref. [26].

Figure 6 shows μ/T dependence of n_q/T^3 at $T = 0.93T_{c0}$. The definition of lines is the same as in Fig. 5. The difference between two results of g_F^1 and g_F^2 reduces as T decreases from $0.99T_{c0}$ to $0.93T_{c0}$. The extrapolation of g_F^2 thus becomes more reliable as T decreases. As mentioned above, the g_F^2 extrapolation is reliable at least at $\mu/T < 0.8$ for $T = 0.99T_{c0}$. This means that also for $T = 0.93T_{c0}$ the g_F^2 extrapolation is reliable at least at $\mu/T < 0.8$.

Next we consider the case of $T > T_{RW}$. As the extrapolation function from imaginary μ to real μ , we consider g_p^3 and

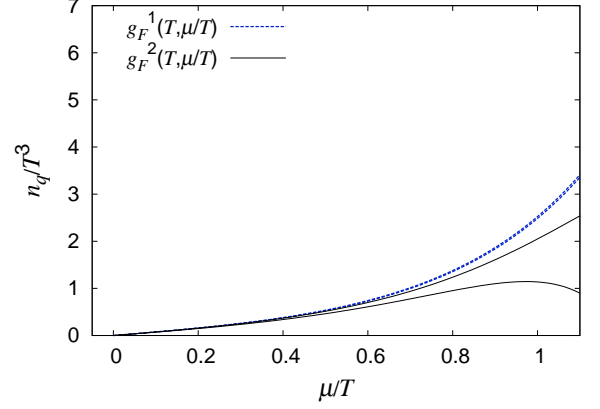


Fig. 6: μ/T dependence of n_q/T^3 at $T = 0.93T_{c0}$. See Fig. 5 for the definition of lines. Two cases of g_F^1 and g_F^2 are plotted.

g_p^5 . Figures 7, 8 and 9 show μ/T dependence of n_q/T^3 at $T = 1.20T_{c0}$, $1.35T_{c0}$ and $2.07T_{c0}$, respectively. The result of g_p^3 (g_p^5) is plotted by a pair of dashed (solid) lines; the two lines correspond to the upper and lower bounds of extrapolation. For each temperature, the result of g_p^3 agrees with the previous result [26] of the Taylor expansion method for the reweighting factor. In the Taylor expansion method, n_q is described by a polynomial series and the terms up to $(\mu/T)^3$ are taken. The highest order taken is the same between the g_p^3 extrapolation and the Taylor expansion method. The agreement of n_q between the two methods is thus natural, although the coefficients are determined with different procedures between the two methods. The difference between g_p^3 and g_p^5 becomes small as T increases. Contributions of order higher than $(\mu/T)^3$ thus become small as T increases.

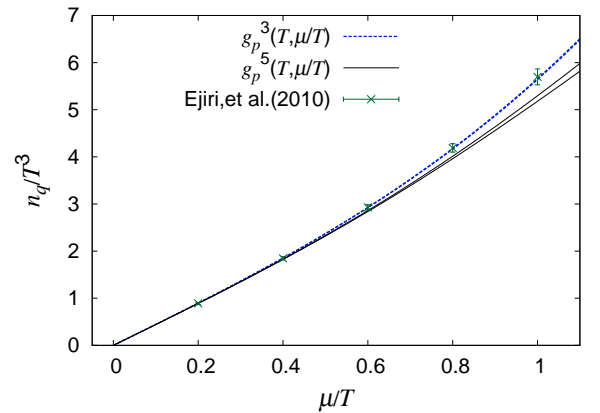


Fig. 7: μ/T dependence of n_q/T^3 at $T = 1.20T_{c0}$. Two cases of g_p^3 and g_p^5 are plotted. The upper and the lower bounds of χ^2 fitting are shown by a pair of dashed lines for g_p^3 and by a pair of solid lines for g_p^5 . The symbols denotes LQCD results of the Taylor expansion method for the reweighting factor in Ref. [26].

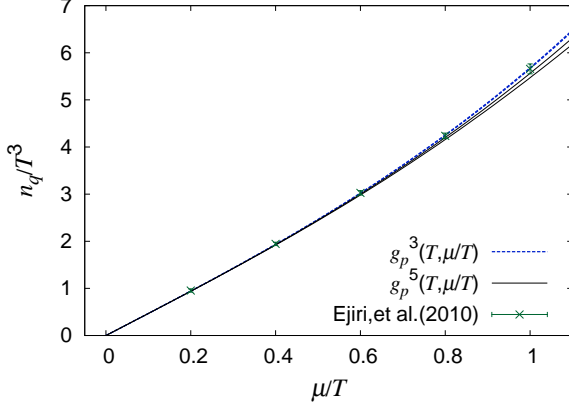


Fig. 8: μ/T dependence of n_q/T^3 at $T = 1.35T_{c0}$. Two cases of g_p^3 and g_p^5 are plotted. See Fig. 7 for the definition of lines. The symbols denotes LQCD results of the Taylor expansion method for the reweighting factor in Ref. [26].

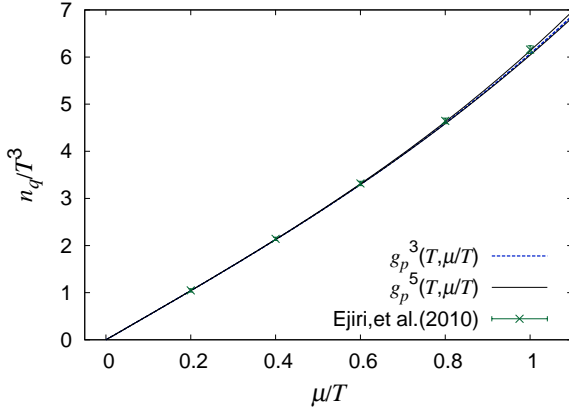


Fig. 9: μ/T dependence of n_q/T^3 at $T = 2.07T_{c0}$. Two cases of g_p^3 and g_p^5 are plotted. See Fig. 7 for the definition of lines. The symbols denotes LQCD results of the Taylor expansion method for the reweighting factor in Ref. [26].

Now we estimate the upper bound $(\mu/T)_{\max}$ of the region in which the extrapolation is considered to be reliable, and investigate T dependence of $(\mu/T)_{\max}$ for $T > T_{RW}$. For this purpose, we define the relative difference δ between g_p^3 and g_p^5 as $\delta = |g_p^5 - g_p^3|/g_p^5$, and assume that the extrapolation is reliable when $\delta < 0.1$. The relative difference δ exceeds 10% at $\mu/T \simeq 0.72$ for $T = 1.20T_{c0}$, $\mu/T \simeq 1.2$ for $T = 1.35T_{c0}$ and $\mu/T \simeq 2.6$ for $T = 2.07T_{c0}$, as shown in Fig. 10. The upper bound $(\mu/T)_{\max}$ of the reliable extrapolation is plotted as a function of T/T_{c0} in Fig. 11. The upper bound goes up as T increases, indicating that contributions of order higher than $(\mu/T)^3$ become less important as T becomes high. Thus the present result of g_p^3 and the previous result [26] of the Taylor expansion method become more reliable as T increases.

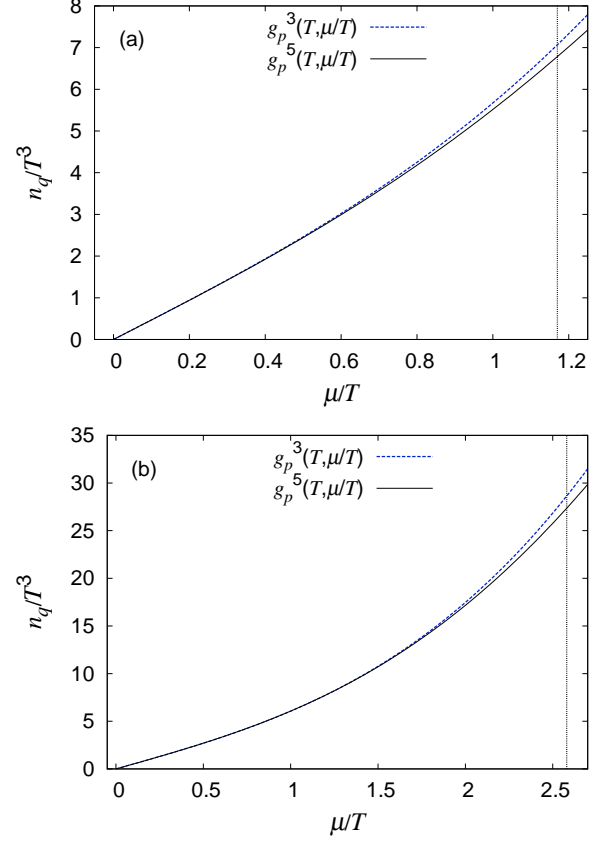


Fig. 10: μ/T dependence of n_q/T^3 and the region of $\delta \leq 0.1$ for (a) $T = 1.35T_{c0}$ and (b) $T = 2.07T_{c0}$. The relative difference δ exceeds 10% at $\mu/T = (\mu/T)_{\max}$ represented by the vertical dotted line. The dashed and solid lines denote the mean values of g_p^3 and g_p^5 , respectively.

IV. HADRON RESONANCE GAS MODEL

Now we consider the confinement region at $\theta \geq 0$, and test whether nucleon and Δ -resonance masses can be determined from the present LQCD results at $\theta \geq 0$ by using the HRG model particularly in the vicinity of T_{c0} . The HRG model considers non-interacting hadrons and resonances, each classified with species i , i.e., with mass m_i , baryon number B_i and isospin I_{3i} . For the 2+1 flavor case at zero chemical potential, the HRG model well reproduces LQCD data on pressure at $T < 1.2T_{c0}$ [30]. This means that the HRG model is applicable at $T < T_{c0}$ even if θ is finite, because $T_c(\theta) > T_{c0}$ for any finite θ . The pressure of the model is obtained by

$$p^{\text{HRG}} = -\frac{T}{V} \sum_{i \in \text{meson}} \ln Z_i^{\text{M}}(T, V, \mu_i) - \frac{T}{V} \sum_{i \in \text{baryon}} \ln Z_i^{\text{B}}(T, V, \mu_i) \quad (14)$$

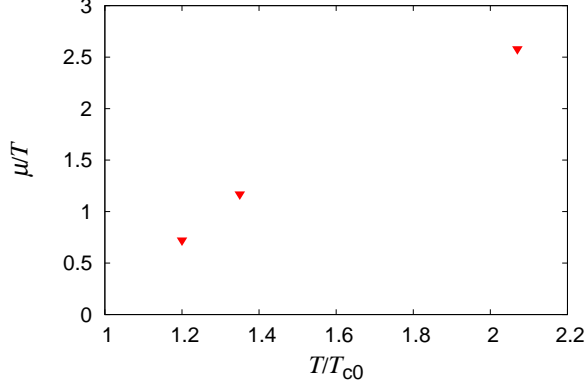


Fig. 11: T dependence of the upper bound $(\mu/T)_{\max}$ of the reliable extrapolation for the case of $T > T_{\text{RW}}$.

with

$$\ln Z_i^{\text{M/B}} = \pm \frac{V g_i}{2\pi^2} \int_0^\infty dp p^2 \ln \left(1 \mp z_i e^{-\epsilon_i/T} \right) \quad (15)$$

for the energy $\epsilon_i = \sqrt{p^2 + m_i}$, the degeneracy factor g_i and the fugacity

$$z_i = e^{\mu_i/T} = \exp \left(\frac{B_i \mu_B + 2I_{3i} \mu_{\text{iso}}}{T} \right), \quad (16)$$

where $\mu_B (\equiv 3\mu)$ and μ_{iso} are the baryon and isospin chemical potentials, respectively. Here we consider only the case of $\mu_{\text{iso}} = 0$. The baryon number density is easily obtained as

$$n_B^{\text{HRG}} = -\frac{\partial}{\partial \mu_B} p^{\text{HRG}}. \quad (17)$$

There are lattice artifacts in LQCD simulations. These were already discussed in Refs. [25, 26, 39–41]. For small N_t , for example, thermodynamic quantities exceed the Stefan-Boltzmann (SB) limit. Since it is not easy to eliminate the lattice artifact exactly, we take the following simple prescription. We consider the lattice SB limit that is defined by the lattice action with massless and free quarks, and normalize LQCD results with the corresponding values in the lattice SB limit in order to reduce the lattice artifacts; see Appendix A for the quark number density in the lattice SB limit. For the HRG model, meanwhile, the quark number density is normalized by the value in the continuum SB limit. In the HRG model, we assume that nucleon mass m_N and Δ -resonance mass m_Δ depend on T only. The baryon masses are determined so as to reproduce the LQCD result. Here we assume that the masses of 24 resonance states above the mass threshold m_{cut}^B are fixed at 1.8 GeV, following Ref. [39]. But the contribution of 24 states to n_q is small.

Figure 12 shows θ dependence of the normalized quark number density n_q/n_{SB} for $T = 0.93T_{c0}$ and $0.99T_{c0}$. The HRG-model results (solid lines) well reproduce θ dependence

of LQCD results (symbols with error bars) for both cases of $T = 0.93T_{c0}$ and $0.99T_{c0}$. This implies that m_N and m_Δ little depend on θ . The resulting nucleon and Δ -resonance masses are shown in Table IV, together with $\chi^2/\text{d.o.f.}$ values. The $\chi^2/\text{d.o.f.}$ values are close to those for g_F^2 in Table II. The resulting masses are heavier than the corresponding physical values, because the quark mass is much heavier than the physical value in our simulations. As shown in Table IV, both m_N and m_Δ decrease by about 10% as T increases from $0.93T_{c0}$ to $0.99T_{c0}$.

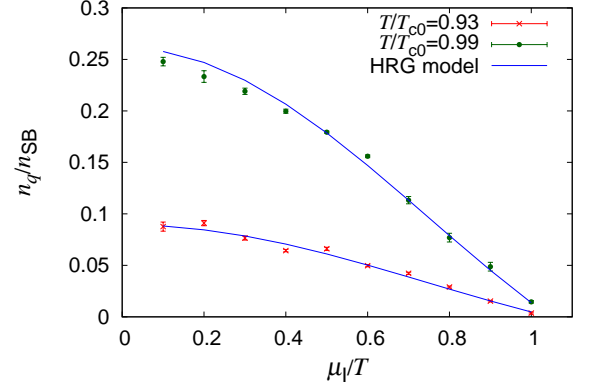


Fig. 12: θ dependence of n_q/n_{SB} at $T = 0.93T_{c0}$ and $0.99T_{c0}$. The cross and square symbols with error bars represent the LQCD results at $T = 0.93T_{c0}$ and $0.99T_{c0}$, respectively, whereas the solid lines stand for the HRG model results.

T/T_{c0}	m_N	m_Δ	$\chi^2/\text{d.o.f.}$
0.93	1091 MeV	1547 MeV	6.625
0.99	940 MeV	1385 MeV	7.993

TABLE IV: Results of χ^2 fitting for baryon masses m_N and m_Δ in the HRG model and $\chi^2/\text{d.o.f.}$ values.

Finally we consider the case of real μ . The HRG model becomes less reliable as μ increases, because the pseudocritical temperature $T_c(\mu)$ of deconfinement transition goes down from T_{c0} as μ increases from zero. Figure 13 shows the μ/T dependence of n_q/n_{SB} at $T = 0.99T_{c0}$. In the range $\mu/T < 0.4$, the HRG model result (solid line) is consistent with the previous LQCD results [26] (symbols with error bars) based on the Taylor expansion method for the reweighting factor. Beyond the range, the HRG model overestimates the LQCD results. The HRG model is thus reliable only at $\mu/T < 0.4$ for the case of $T = 0.99T_{c0}$.

V. SUMMARY

We have investigated μ dependence of n_q at imaginary and real μ , performing LQCD simulations at imaginary μ and ex-

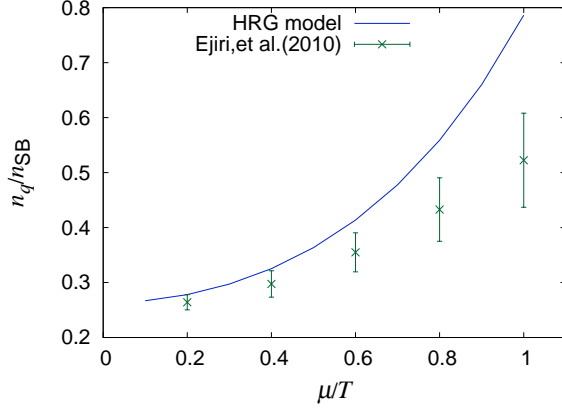


Fig. 13: μ/T dependence of n_q/n_{SB} in the real μ region for $T = 0.99T_{c0}$. The symbols with error bars stand for LQCD results of the Taylor expansion method for the reweighting factor in Ref. [26], while the solid line is the result of the HRG model.

trapolating the results to the real- μ region by assuming functional forms for n_q . LQCD calculations were done on an $8^2 \times 16 \times 4$ lattice with the clover-improved two-flavor Wilson fermion action and the renormalization-group-improved Iwasaki gauge action. We considered two temperatures below T_{c0} and four temperatures above T_{c0} . The quark number density was computed along the line of constant physics at $m_{\text{PS}}/m_V = 0.80$.

For imaginary μ , the quark number density calculated with the Wilson-type fermion action is consistent with the previous result [29] based on the staggered-type fermion action. The LQCD results thus do not depend on the fermion action taken.

We have extrapolated n_q at imaginary μ to real μ , assuming the Fourier series g_F^n for $T < T_{c0}$ and the polynomial series g_p^{2n-1} for $T > T_{\text{RW}}$; here the superscript n represents the highest order in the partial sum. As for $T = 0.99T_{c0}$, the present result of g_F^2 is consistent with the previous result [26] of the Taylor expansion method for the reweighting factor in the range $\mu/T < 0.8$. The extrapolation based on g_F^2 is thus reliable at $\mu/T < 0.8$ for $T = 0.99T_{c0}$. Furthermore, the difference between the two results of g_F^1 and g_F^2 reduces as T decreases from T_{c0} , indicating that higher-order contributions become less important as T decreases. Therefore, the extrapolation based on g_F^2 is reliable at $\mu/T < 0.8$ for any T less than T_{c0} .

For $T > T_{\text{RW}}$, the previous study based on the Taylor expansion method for the reweighting factor has contributions up to $(\mu/T)^3$, but the present g_p^5 extrapolation retains contributions up to $(\mu/T)^5$. Using this advantage of the present method from the previous method, we have estimated to what extent the Taylor expansion or the g_p^3 extrapolation works. The upper bound $(\mu/T)_{\text{max}}$ of the reliable extrapolation goes up as T increases from T_{RW} , because higher-order contributions become less important.

The HRG model is reliable in the confinement region. For

the 2+1 flavor case at zero chemical potential, in fact, the HRG model well reproduces LQCD data on pressure at $T < 1.2T_{c0}$ [30]. When μ is varied with T fixed at T_{c0} , the system is in the confinement phase at imaginary μ but in the deconfinement phase at real μ . This means that the HRG model is more reliable at imaginary μ than at real μ , when T is fixed at T_{c0} . We have then tested whether T dependence of m_N and m_Δ in the vicinity of T_{c0} can be determined from LQCD data on n_q at imaginary μ by using the HRG model. The HRG model well reproduces the LQCD results, when m_N and m_Δ are assumed to depend on T only. This implies that m_N and m_Δ little depend on $\theta (= \mu_I/T)$. In our test calculation, m_N and m_Δ reduce by about 10% when T increases from $0.93T_{c0}$ to $0.99T_{c0}$. We propose this method as a handy way of determining T dependence of m_N and m_Δ in the vicinity of T_{c0} . This method is practical, since it is not easy to measure T dependence of pole masses directly with LQCD simulations.

Acknowledgments

We thank A. Nakamura and K. Nagata for useful discussions and giving the LQCD program codes. We are also grateful to I.-O. Stamatescu, T. Sasaki and T. Saito for helpful discussions. J. T., H. K., and M. Y. are supported by Grant-in-Aid for Scientific Research (No. 25-3944, No. 26400279 and No. 26400278) from the Japan Society for the Promotion of Science (JSPS). The numerical calculations were performed on NEC SX-9 and SX-8R at CMC, Osaka University and on HITACHI HA8000 at Research Institute for Information Technology, Kyushu University.

Appendix A: Quark number density for the Wilson fermion in the massless free-gas limit

We consider n_q for the Wilson fermion in the lattice SB limit (the massless free-gas limit). In the high- T limit, we can consider a quark as a massless and non-interacting particle, since the effects of finite quark mass and interactions between quarks are negligible there. In Appendix of Ref. [26], the lattice SB limit is discussed except for the quark number density.

The partition function with free Wilson fermions is given by

$$Z(\kappa, \hat{\mu}) = (\det M)^{N_f}, \quad (\text{A1})$$

$$M_{xy} = \delta_{xy} - \kappa \sum_{i=1}^3 \left[(1 - \gamma_i) \delta_{x+\hat{i}, y} + (1 + \gamma_i) \delta_{x-\hat{i}, y} \right] - \kappa \left[e^{+\hat{\mu}} (1 - \gamma_4) \delta_{x+\hat{4}, y} + e^{-\hat{\mu}} (1 + \gamma_4) \delta_{x-\hat{4}, y} \right], \quad (\text{A2})$$

on an $N_x \times N_y \times N_z \times N_t$ lattice. After the unitary transfor-

mation to momentum space, we obtain

$$Z(1/8, \hat{\mu}) = \left(\prod_k \det \tilde{M}(k) \right)^{N_c N_f} \quad (\text{A3})$$

$$\det \tilde{M}(k) = \frac{16}{8^4} \left[\sum_i \sin^2 k_i + \left\{ 2 \sum_i \sin^2 \left(\frac{k_i}{2} \right) \right\}^2 + 4 \left\{ 2 \sum_i \sin^2 \left(\frac{k_i}{2} \right) + 1 \right\} \sin^2 \left(\frac{k_t - i\hat{\mu}}{2} \right) \right]^2 \quad (\text{A4})$$

in the massless quark limit $\kappa = 1/8$, where \tilde{M} is the fermion matrix in momentum space, and

$$k_i = \frac{2\pi j_i}{N_i}, \quad j_i = 0, \pm 1, \dots, N_i/2 \quad (\text{A5})$$

for the spatial components ($i = x, y, z$) and

$$k_t = \frac{2\pi(j_t + 1/2)}{N_t}, \quad j_t = 0, \pm 1, \dots, N_t/2 \quad (\text{A6})$$

for the time component. The quark number density in the lattice SB limit is then obtained as

$$\begin{aligned} \frac{n_q}{T^3} &= \frac{N_t^3}{N_V} \frac{\partial}{\partial \hat{\mu}} \ln Z(1/8, \hat{\mu}) \\ &= N_c N_f \frac{N_t^3}{N_V} \sum_k \frac{\partial \det \tilde{M}(k)}{\partial \hat{\mu}} [\det \tilde{M}(k)]^{-1} \quad (\text{A7}) \end{aligned}$$

$$\begin{aligned} \frac{\partial \det \tilde{M}(k)}{\partial \hat{\mu}} &= -\frac{1}{8^2} \left\{ 2 \sum_i \sin^2 \left(\frac{k_i}{2} \right) + 1 \right\} \\ &\quad \times (\sinh \hat{\mu} \cos k_t + i \cosh \hat{\mu} \sin k_t). \quad (\text{A8}) \end{aligned}$$

The quark-number density at imaginary μ is obtained by replacing $\hat{\mu}$ by $i\hat{\mu}_I$ in Eqs. (A7) and (A8).

-
- [1] P. B. Demorest, T. Pennucci, S. M. Ransom, M. S. E. Roberts, and J. W. T. Hessels, *Nature* **467**, 1081 (2010).
 - [2] L. Kumar (for the STAR Collaboration), *Nucl. Phys. A*, **904**, 256c, (2013).
 - [3] E. O'Brien (for the PHENIX Collaboration), *Nucl. Phys. A*, **904**, 264c, (2013).
 - [4] S. Muroya, A. Nakamura, C. Nonaka, and T. Takaishi, *Prog. Theor. Phys.* **110**, 615 (2003).
 - [5] P. de Forcrand, *Proc. Sci., LAT2009*, **010**, arXiv:1005.0539 [hep-lat], (2009).
 - [6] G. Aarts, *Phys. Rev. Lett.* **102**, 131601 (2009).
 - [7] G. Aarts, L. Bongiovanni, E. Seiler, D. Sexty, and I. -O. Stamatescu, *Eur. Phys. J. A* **49**, 89 (2013).
 - [8] D. Sexty, *Phys. Lett. B* **729**, 108 (2014).
 - [9] G. Aarts, E. Seiler, D. Sexty, and I. -O. Stamatescu, arXiv:1408.3770 [hep-lat], (2014).
 - [10] M. Cristoforetti, F. DiRenzo, and L. Scorzato, *Phys. Rev. D* **86**, 074506 (2012).
 - [11] H. Fujii, D. Honda, M. Kato, Y. Kikukawa, S. Komatsu, and T. Sano, *J. High Energy Phys.* **10**, 147 (2013).
 - [12] A. Roberge, and N. Weiss, *Nucl. Phys.* **B275**, 734 (1986).
 - [13] Y. Aoki, G. Endrödi, Z. Fodor, S. D. Katz, and K. K. Szabó, *Nature* **443**, 675 (2006).
 - [14] H. Kouno, Y. Sakai, K. Kashiwa, and M. Yahiro, *J. Phys. G* **36**, 115010 (2009) [arXiv:0904.0925 [hep-ph]].
 - [15] P. de Forcrand, and O. Philipsen, *Nucl. Phys.* **B642**, 290 (2002).
 - [16] L.-K. Wu, X.-Q. Luo, and H.-S. Chen, *Phys. Rev. D* **76**, 034505 (2007).
 - [17] M. D'Elia, and M.-P. Lombardo, *Phys. Rev. D* **67**, 014505 (2003).
 - [18] M. D'Elia, and M.-P. Lombardo, *Phys. Rev. D* **70**, 074509 (2004).
 - [19] P. de Forcrand, and O. Philipsen, *Phys. Rev. Lett.* **105**, 152001 (2010).
 - [20] K. Nagata, and A. Nakamura, *Phys. Rev. D* **83**, 114507 (2011).
 - [21] Y. Sakai, K. Kashiwa, H. Kouno and M. Yahiro, *Phys. Rev. D* **77**, 051901 (2008) [arXiv:0801.0034 [hep-ph]].
 - [22] Y. Sakai, T. Sasaki, H. Kouno, and M. Yahiro, *J. Phys. G* **39**, 035004 (2012).
 - [23] Y. Sakai, K. Kashiwa, H. Kouno, M. Matsuzaki, and M. Yahiro, *Phys. Rev. D* **78**, 076007 (2008).
 - [24] J. Sugano, J. Takahashi, M. Ishii, H. Kouno and M. Yahiro, *Phys. Rev. D* **90**, 037901 (2014).
 - [25] C. R. Allton, S. Ejiri, S. J. Hands, O. Kaczmarek, F. Karsch, E. Laermann, and C. Schmidt, *Phys. Rev. D* **68**, 014507 (2003).
 - [26] S. Ejiri et al. (WHOT-QCD Collaboration), *Phys. Rev. D* **82**, 014508 (2010).
 - [27] M. D'Elia, F. DiRenzo, and M. P. Lombardo, *Phys. Rev. D* **76**, 114509 (2007).
 - [28] P. Cea, L. Cosmai, M. D'Elia and A. Papa, *JHEP* **02**, 066 (2007).
 - [29] M. D'Elia, and F. Sanfilippo, *Phys. Rev. D* **80**, 014502 (2009).
 - [30] S. Borsanyi, G. Endrodi, Z. Fodor, S. D. Katz, S. Krieg, C. Ratti, and K. K. Szabo, *JHEP* **1208**, 053 (2012) [arXiv:1204.6710 [hep-lat]].
 - [31] A. Ali Khan et al. (CP-PACS Collaboration), *Phys. Rev. D* **63**, 034502 (2000).
 - [32] Y. Iwasaki, *Nucl. Phys.* **B258**, 141 (1985).
 - [33] B. Sheikholeslami, and R. Wohlert, *Nucl. Phys.* **B259**, 572 (1985).
 - [34] A. Ali Khan et al. (CP-PACS Collaboration), *Phys. Rev. D* **64**, 074510 (2001).
 - [35] Y. Maezawa et al. (WHOT-QCD Collaboration), *Phys. Rev. D* **75**, 074501 (2007).
 - [36] P. Cea, L. Cosmai, M. D'Elia, and A. Papa, *Phys. Rev. D* **77**, 051501 (2008).
 - [37] P. Cea, L. Cosmai, M. D'Elia, C. Manneschi, and A. Papa, *Phys. Rev. D* **80**, 034501 (2009).
 - [38] P. Cea, L. Cosmai, M. D'Elia, and A. Papa, *Phys. Rev. D* **81**, 094502 (2010).

- [39] P. Huovinen, and P. Petreczky, Nucl. Phys. A **837**, 26 (2010).
- [40] O. Philipsen, and L. Zeidlewicz, Phys. Rev. D **81**, 077501 (2010).
- [41] A. Bazavov et al. (HotQCD Collaboration), Phys. Rev. D **85**, 054503 (2012).